Cell Biochemistry and Biophysics
https://doi.org/10.1007/s12013-024-01429-z

ORIGINAL PAPER

Effect of Xanthohumol from *Humulus lupulus* L. Against Gouty Bone Damage in Arthritis of Rats Induced by Mono-sodium Urate

Jianyong Han[1,2] · Tianshuang Xia[1] · Yiping Jiang[1] · Weiqing Fan[3] · Nani Wang[4] · Yue Zhang[1] · Aijun Liu[1,5] · Kai Zhao[6] · Hailiang Xin[1]

Accepted: 11 July 2024

Abstract

Xanthohumol (XAN) is an isoprenyl flavonoid from *Humulus lupulus* L. known for beer brewing, and an osteoprotective agent due to its active improvement in bone loss of osteoporosis. This study was first time to investigate its effects on anti-gouty bone injury in rats of gouty arthritis (GA) induced by monosodium urate (MSU). Results showed that XAN could significantly exert anti-inflammatory activity by alleviating swelling degree of joints, reducing serum level of inflammatory factors, improving inflammatory injury and degrading the Markin's score in lesion joint. Meanwhile, XAN could also fight against gouty bone damage by improving pathological changes of bone tissue and parameters of bone micro-structure. Moreover, XAN could even promote bone formation by effectively enhancing expression of Runx2 and OPG, while inhibit bone resorption with depressing matrix metalloproteinase-9 (MMP-9), MMP-13 and CTSK expression, reducing RANKL secretion, and abating the ratio of RANKL/OPG. Therefore, it was the first time to reveal the mechanism of XAN against gouty bone injury via inhibiting RANKL/OPG/RANK signaling pathway. Above all, this study provided potential strategy for the treatment of GA, and further contributed to research and resource development for hops.

Keywords Xanthohumol · *Humulus lupulus* L. · Gouty bone damage · Gouty arthritis · Monosodium urate

Introduction

Clinically, GA is a crystal-related disease usually characterized as redness, overt swelling, severe pain, synovium hyperplasia, inflammatory infiltration, joint degeneration and dysfunction, cartilage injury and even bone erosion in the lesion joints induced by the accumulation of deposited MSU [1]. According to epidemiological statistics, the rate of GA incidence is about 5%, and 80% of patients relapse within 3 years [2]. What's more, in chronic GA, 44% of individuals commonly suffer from a lower quality of life with acute episodes of arthritis, chronic gouty bone damage and physical disability in severe cases [3]. Currently, drugs in clinical first-line for GA are etoricoxib (ETO), allopurinol, colchicine, and glucocorticoids, which are beneficial for relieving inflammation and pain [4]. However, there are few medications for gouty bone damage or bone erosion [5]. Therefore, safe and novel medicines for the regulation of bone metabolism in GA are urgently needed.

The monomer components of flavonoids in Chinese herbal medicines used for gout commonly have multi

These authors contributed equally: Jianyong Han, Tianshuang Xia

✉ Hailiang Xin
hailiangxin@163.com

[1] School of Pharmacy, Naval Medical University, Shanghai 200433, China

[2] Outpatient Department of PLA Unit 92919, Ningbo, Zhejiang 315000, China

[3] Yueyang Hospital of Integrated Traditional Chinese and Western Medicine, Shanghai University of Traditional Chinese Medicine, Shanghai 200433, China

[4] Department of Medicine, Zhejiang Academy of Traditional Chinese Medicine, Hangzhou, Zhejiang 310007, China

[5] Department of Pharmacy Research, Yueyang Hospital of Integrated Traditional Chinese and Western Medicine, Shanghai University of Traditional Chinese Medicine, Shanghai 200437, China

[6] Hebei Kingsci Pharmaceutical Technology, Shijiazhuang 050035, China

Published online: 21 July 2024

activities against gouty signs and symptoms [6–11]. *Humulus lupulus* L. is a perennial vine plant with female flower ears [12], which is used for beer brewing. It can also be applied to treat hot flashes during menopause and post-menopausal osteoporosis [13, 14]. Xanthohumol (XAN) is an isoprenyl flavonoid from hops, and has active effects with anti-inflammation, anti-oxidation, anti-tumor and anti-osteoporosis [15–17]. Moreover, XAN does not impair organ function and homeostasis in the range of safe drug dose as long term use, which was safe and well-tolerated without side effects according to toxicology researches [18–20]. Our previous researches have already confirmed its regulation on serum uric acid level and bone metabolism in hyperuricemia rats [21], and its effects on bone homeostasis in osteoporosis model [22–26]. In this study, it was the first time to investigate anti-inflammatory and anti-gouty bone injury effects of XAN on GA, and explore its potential mechanism against gouty bone damage, in order to provide reference for development of new anti-gout drugs.

Materials and Methods

Instruments and Reagents

MSU crystals were prepared by recrystallizion of uric acid (U0881, Sigma, USA) according to the reference [27], and collected after sterilization. Clusters of MSU crystals like needle tip were fine for the following experiment with a length between 25 and 100 μm. The MSU crystals were suspended into 50 mg/ml with phosphate buffered saline (PBS) for intra-articular injection (i.a.). XAN (Purity (HPLC) ≥ 99.0%, 8065102, Li Ding, China) and ETO (H20210036, Merck Sharp, Australia) were dissolved with 0.5% CMC-Na (MB1731, Meilunbio, China) for intragastric administration. In addition, the interleukin-1β (IL-1β, H002-1-2), interleukin-6 (IL-6, H007-1-2), tumor necrosis factor-α (TNF-α, H052-1-2), and prostaglandin e2 (PGE2, H099-1-2) were tested with enzyme-linked immunosorbent assay (ELISA) kits were purchased from Jiancheng Bioengineering Institute (Nanjing, China). Chloral hydrate (C46249, Macklin) and 4% paraformaldehyde (BL539A, Beyotime) were obtained from Beyotime Biotechnology Co., Ltd (Shanghai, China). Primary antibodies for cathepsin K (CTSK, DF6614), matrix metalloproteinase-9 (MMP-9, AF5228), MMP-13 (AF5355), runt-related transcription factor 2 (Runx2, AF5186), receptor activator of nuclear factor kappa-B (NF-κB) ligand (RANKL, AF0313) and osteoprotegerin (OPG, DF6824) were bought from Affinity Bioscience Co., Ltd (Jiangsu, China). Secondary antibodies fluorescence-labeled with horseradish peroxidase (HRP) of anti-rabbit IgG (ZC-G2107), and 488 anti-rabbit IgG (ZC-G2503) were purchased from Zcibio Technology CO., LTD (Shanghai, China).

Animals and Treatment

50 male Wistar rats (body weight 180 ± 20 g) were purchased from Shanghai Laboratory of Family Planning Science Institute (Certificate No.: 20220006041877; License No.: SCXK (Shanghai) 2022-0006). All rats were reared in temperature-controlled room (24 ± 1 °C) of the Laboratory Animal Center of Naval Medical University, with a 12-h light/dark cycle and allowed free to feed and water. All experiments on rats were complied with guidelines for the ethical treatment of animals issued by the Naval Medical University and approved by the Committee on Ethics of Medical Research (approved No. 202102624) on 01-02-2021.

Experimental Design

GA model was induced by 50 μl MSU suspension (50 mg/ml) injected into the ankle cavity of left hind limb once for every three days according to the reference [28]. Furthermore, the doses for XAN were selected according to our previous study [23], and ETO referred to the related paper [28]. Rats were randomly and equally divided into 5 groups ($n = 10$): control group (CON; 50 μl PBS, i.a. q3d; 0.5% CMC-Na, i.g. qd), model group (MOD; 50 μl MSU, i.a. q3d; 0.5% CMC-Na, i.g. qd), ETO group (ETO; 50 μl MSU, i.a. q3d; ETO 18 $mg{\cdot}kg^{-1}{\cdot}d^{-1}$, i.g), XAN low dose group (XAN-L; 50 μl MSU, i.a. q3d; XAN 15 $mg{\cdot}kg^{-1}{\cdot}d^{-1}$, i.g.), and XAN high dose group (XAN-H; 50 μl MSU, i.a. q3d; XAN 45 $mg{\cdot}kg^{-1}{\cdot}d^{-1}$, i.g). The dosage for gavage administration was adjusted according to the weight of rat per week. All rats were treated continuously for 10 weeks.

Ankle Swelling

To assess swelling degree of rat's ankle, diameters of both left and right hind limbs (i.e., SL and SR) were measured by vernier caliper (P2394689, Liang Ju, China) once per week, with same horizontal position selected at level of internal to lateral joint lines for each measurement. The ankle swelling was converted according to formula S= (SL - SR) / SR× 100%.

Sample Collection and Detection

Rats were anesthetised with 10% chloral hydrate via intraperitoneal injection. Blood samples were obtained from abdominal aorta, and 2 h later, serum samples were collected via centrifuge at 5810 × *g* for 10 min. The levels of IL-1β, IL-6, TNF-α, and PGE2 were detected according to

Table. 1 Effects of XAN on ankle swelling in GA rats $(\%, n = 10, \bar{x} \pm s)$

Week	CON	MOD	ETO	XAN-L	XAN-H
1st	0.08 ± 0.16	4.58 ± 1.11**	1.39 ± 0.56ΔΔ	3.15 ± 1.27ΔΔ	1.97 ± 0.53ΔΔ
2nd	0.11 ± 0.18	7.05 ± 0.98**	1.90 ± 0.51ΔΔ	4.13 ± 1.07ΔΔ	2.56 ± 0.65ΔΔ
3rd	0.15 ± 0.19	8.88 ± 1.02**	2.45 ± 0.54ΔΔ	5.16 ± 0.90ΔΔ	3.76 ± 0.60ΔΔ
4th	0.18 ± 0.19	11.32 ± 1.58**	2.88 ± 0.61ΔΔ	6.14 ± 0.78ΔΔ	4.70 ± 0.65ΔΔ
5th	0.22 ± 0.19	13.69 ± 1.69**	3.09 ± 0.59ΔΔ	7.18 ± 1.05ΔΔ	5.36 ± 0.63ΔΔ
6th	0.24 ± 0.17	15.09 ± 1.05**	3.85 ± 0.43ΔΔ	7.99 ± 1.25ΔΔ	5.91 ± 0.76ΔΔ
7th	0.28 ± 0.21	16.12 ± 1.44**	4.34 ± 0.73ΔΔ	8.73 ± 0.90ΔΔ	6.67 ± 1.00ΔΔ
8th	0.30 ± 0.19	17.67 ± 1.45**	5.08 ± 0.80ΔΔ	10.13 ± 0.94ΔΔ	7.84 ± 1.16ΔΔ
9th	0.36 ± 0.18	19.56 ± 1.18**	5.59 ± 0.51ΔΔ	11.02 ± 0.89ΔΔ	8.66 ± 1.04ΔΔ
10th	0.42 ± 0.15	21.07 ± 2.27**	6.11 ± 0.95ΔΔ	12.43 ± 1.62ΔΔ	10.36 ± 0.81ΔΔ

**$P < 0.01$ vs control group; ΔΔ$P < 0.01$ vs model group

Table. 2 Effects of XAN on levels of inflammatory factors in serum $(\mu mol \cdot L^{-1}, n = 10, \bar{x} \pm s)$

	CON	MOD	ETO	XAN-L	XAN-H
IL-1β	6.96 ± 0.50	9.26 ± 1.34**	6.29 ± 0.95ΔΔ	5.70 ± 1.04ΔΔ	6.07 ± 1.22ΔΔ
IL-6	3.65 ± 1.17	11.68 ± 4.06**	5.24 ± 2.20ΔΔ	4.21 ± 2.25ΔΔ	5.90 ± 1.25ΔΔ
TNF-α	52.64 ± 28.06	351.32 ± 173.30**	123.25 ± 26.71ΔΔ	210.78 ± 32.03ΔΔ	171.12 ± 32.30ΔΔ
PGE2	58.91 ± 25.53	249.02 ± 61.11**	89.34 ± 22.25ΔΔ	149.89±26.74ΔΔ▲▲	114.26 ± 37.34ΔΔ

IL-1β interleukin-1 bata, *IL-6* interleukin-6, *PGE2* prostaglandin e2, *TNF-α* tumor necrosis factor- α

**$P < 0.01$ vs CON group; ΔΔ$P < 0.01$ vs MOD group; ▲▲$P<0.01$ vs ETO group

kit's instructions Table 1, 2. The left posterior ankle joints were isolated and fixed in 4% paraformaldehyde, and then used for Mirco-CT detection, pathological section staining, immunohistochemical staining and immunofluorescence detection.

Pathological Histomorphologic Evaluation

Rat's ankle joints fixed in 4% paraformaldehyde were transferred to deccalcification solution. After decalcification at room temperature for 14 days, embedding medium was added and placed in –20 °C for frozen section. Hemoxylin eosin (HE), safranin O / fast green (SO) and tartrate resistant acid phosphatase (TRAP) staining were respectively used and observed under an inverted fluorescence microscope (CKX 53, OLYMPUS, Japan). For tissue sections stained with HE and SO, five different fields were randomly selected to evaluate degree of inflammatory damage by Mankin's score, with mild (0–3); moderate (4–9); and severe (10–14) [29]. The number of TRAP positive cells were analyzed from five randomly selected fields of view each time.

Micro-CT Scanning and 3D Micro-structural Analysis

The specimens of entire ankle joints were scanned via a high-resolution animal micro focal computed tomography (micro-CT) scanner (Explore Locus-SP, GE, USA). Corresponding settings were as below: X-ray tube voltage (60 kVp); tube current (200 μAs); exposure time (3000 ms); projection number (1000); and voxel size (8 μm). The plane and 3-dimensional (3D) reconstructions of rat's ankle were obtained by Micview V2.1.2 software. Furthermore, a cuboid of trabecular bone at the top of fibula with a size of $1.5 \times 1.5 \times 1.5\ mm^3$ was selected as the region of interest (ROI) for quantitative analysis of bone micro-architecture parameters.

Immunohistochemical (IHC) Staining

Sections were separately incubated overnight with prepared primary antibodies including anti-CTSK, anti-MMP-9, anti-MMP-13 and anti-Runx2 (dilution 1:100 *v/v*) at 4 °C, and then with corresponding secondary antibodies (dilution 1:1000 *v/v*) for 30 min at room temperature. Finally, positive cells were stained with brownish yellow and quantified by Image J with five randomly selected fields under an inverted fluorescent microscope at each time, so the positive cells and signal area in the IHC staining images were then performed for downstream statistical analysis [30].

Double-labeling Immunofluorescent Detection

For double-labeling immunofluorescent staining of RANKL and OPG, paraffin sections were incubated with primary antibodies of RANKL (1:2000 *v/v*) that were diluted with blocking buffer at 4 °C overnight. In the next day, the slides were incubated with corresponding secondary antibodies

fluorescence-labeled with HRP anti-rabbit IgG (1:500 *v/v*, red fluorescence) for 50 min at room temperature. After the slices were slightly dried, tyramide signal amplification (TSA) were added in the circle and incubated for 10 min at room temperature. Then, sections were placed in a repair box filled with antigen repair buffer and heated in the microwave oven. Furthermore, step with the previous, sections were performed with primary antibodies of OPG (1:200 *v/v*) and corresponding secondary antibodies fluorescence-labeled with 488 anti-rabbit IgG (1:400 *v/v*, green fluorescence). The nuclei were redyed with 4,6-diamino-2-phenyl indole (DAPI) dye solution and incubated for 10 min at room temperature. The con-focal images were acquired under an inverted fluorescent microscope, and the positive cells and signal area are quantified by Image J with five randomly selected fields at each time [30], then performed for downstream statistical analysis, including RANKL positive in red, OPG positive in green and co-localization of RANKL and OPG positive in violaceous.

Statistical Analysis

All data in this study are expressed as $\overline{x} \pm s$. All statistical analyses were performed by GraphPad Prism 9.0 software and analyzed with Shapiro-Wilk normality test and F-test test for homogeneity of variance. When variance, one-way analysis of variance (One-Way ANOVA) and Newman-Keuls, the data after the homogeneity of variance, and transformed data. The test level (α) is 0.05.

Results

Effects of XAN on Ankle Swelling in GA Rats

The degree of ankle swelling gradually increased to 21.07 ± 2.27% in MOD group at the end of experiment, while 6.11 ± 0.95% in ETO group, 12.43 ± 1.62% in XAN-L group and 10.36 ± 0.81% in XAN-H group (Tab. 1). Obviously, the ankle swelling in MOD group was higher than that in CON group ($P < 0.01$), indicating significant inflammatory reaction in diseased joints of GA rats. The degree of swelling in ETO group and XAN groups were all lower than that in MOD group (all $P < 0.01$), suggesting that XAN could reduce inflammation and had anti-inflammatory effect in GA rats.

Effects of XAN on Serum Level of Inflammatory Cytokines in GA Rats

The levels of IL-1β, IL-6, TNF-α and PGE2 in MOD group were higher than those in CON group (Tab. 2, all $P < 0.01$), indicating that MSU induced inflammatory response in rats and stimulated a large number of inflammatory factors. The levels of IL-1β, IL-6, TNF-α, and PGE2 in ETO and XAN groups were lower than those in MOD group (all $P < 0.01$), suggesting that XAN could abate inflammatory reaction induced by MSU through reducing levels of inflammatory factors in GA rats. Meanwhile, there was no significant difference between XAN groups and ETO group in reduction of inflammatory factors, other than PGE2 in XAN-L group ($P < 0.01$). The above results revealed that XAN had good anti-inflammatory activity in GA rats, and the effect of XAN at high dose was comparable to ETO.

Effects of XAN on Histomorphological Evaluation of Diseased Joints

Compared with CON group, HE staining showed that there were large infiltration of inflammatory cells in diseased tissue and obvious hyperplasia of synovial tissue and uneven joint space in MOD group, indicating inflammatory damage in joints of GA rats (Fig. 1A). Compared with MOD group, the ETO group and XAN groups showed different degrees of improvement, with lower infiltration of inflammatory cells and hyperplasia of synovial tissue, indicating that XAN could improve inflammatory damage caused by MSU. In addition, compared with CON group, SO staining in MOD group showed shallow, uneven cartilage matrix, lower cartilage cells and irregular morphology with disorder, defects, cracks and rough edge on cartilage surface, uneven joint space, and lighter density in subcartilage bone matrix, showing signs of inflammatory damage in cartilage and subchondral bone. Compared with MOD group, the staining of cartilage and subchondral bone were relatively balanced in ETO group and XAN groups, with relatively smooth surface and higher density in subchondral bone, suggesting that XAN could improve pathological changes in articular cartilage and subchondral bone. The Markin's score in MOD group was 9.41 ± 1.01 and much higher than 0.70 ± 0.46 in CON group ($P < 0.01$), indicating severe inflammatory injury induced by MSU (Fig. 1B). The scores in XAN-H group (3.90 ± 0.95), XAN-L group (6.54 ± 1.37) and ETO group (2.34 ± 0.85) were lower than that in MOD group ($P < 0.01$), suggesting that XAN reduced the degree of arthritic injury caused by MSU. In addition, the score of XAN-H group was lower than that of XAN-L group ($P < 0.01$), indicating that effect of XAN on arthritic injury was related to its dosage. The above results showed that XAN had anti-inflammatory effect on arthritic injury in GA rats, and its activity was associated with dosage.

Effects of XAN on Bone Morphology and Parameters of Joints

The diseased ankle joints were scanned by Micro-CT. Compared with CON group, morphology changes of lesion

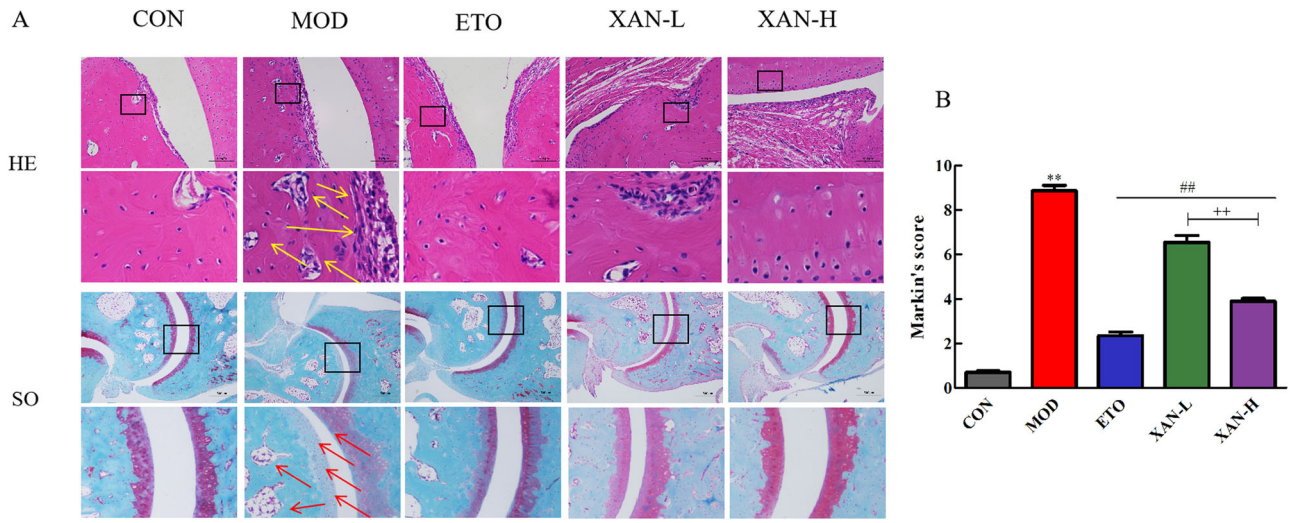

Fig. 1 Effects of XAN on histomorphological evaluation of diseased joints. **A** Numerous inflammatory cells and obvious synovial hyperplasia were indicated with yellow arrows in HE staining. Lighter cartilage matrix, less chondrocytes, larger cavitations in subchondral bone, and lower density of bone matrix were indicated with red arrows in SO staining, scale bars: 100 μm; (**B**) Markin's score. $n = 10$, $\bar{x} \pm s$. $^{**}P < 0.01$ vs. control group; $^{\#\#}P < 0.01$ vs. model group; $^{++}P < 0.01$ vs. XAN-L group. HE hematoxylin-eosin, SO Safranin O/Fast green

site reflected signs of gouty bone injury with uneven surface and cavity, mall trabecular coverage, low density and poor continuity in ROI area of MOD group (Fig. 2A). Meanwhile, BMD (Fig. 2B, $P < 0.01$), BS/TV (Fig. 2C, $P < 0.05$), BV/TV (Fig. 2D, $P < 0.05$), Tb.N. (Fig. 2E, $P < 0.01$) and Conn.Dn (Fig. 2F, $P < 0.01$) in MOD group were lower than those in CON group, while Tb.Sp. (Fig. 2G, $P < 0.01$),Tb.Pf. (Fig. 2H, $P < 0.01$) and SMI (Fig. 2I, $P < 0.01$) were higher, indicating severe damage appeared under long-term stimulation of MSU. Compared with MOD group, bone micro-parameters in XAN-H group and ETO group including BMD (Fig. 2B, $P < 0.01$), BS/TV (Fig. 2C, $P < 0.05$), BV/TV (Fig. 2D, $P < 0.05$), Tb.N. (Fig. 2E, $P < 0.05$) and Conn.Dn (Fig. 2F, $P < 0.05$) elevated, while Tb.Sp. (Fig. 2G, $P < 0.05$), Tb.Pf. (Fig. 2H, $P < 0.01$) and SMI (Fig. 2I, $P < 0.01$) decreased, showing that XAN at high dose could effectively improve bone mineral density and bone micro-parameters of trabecular bone. In addition, bone micro-parameters in XAN-L group including BMD (Fig. 2B, $P < 0.05$), Tb.Sp. (Fig. 2G, $P < 0.05$), Tb.Pf. (Fig. 2H, $P < 0.01$) and SMI (Fig. 2I, $P < 0.01$) were improved, indicating that XAN at low dose could partly regulate structural parameters of diseased bone tissue. The above results revealed that XAN could improve degeneration of bone tissue morphology and changes of bone micro-structure caused by MSU, and had anti-gouty bone injury effect in GA rats, and its effect of improvement may be related to drug dosage.

Effects of XAN on the Differentiation of OC

Compared with CON group, sections in MOD group showed deeper TRAP staining, stronger activity, and more positive cells (Fig. 3B, $P < 0.01$), indicating that MSU caused enhanced TRAP activity and active OC differentiation, leading to bone destruction (Fig. 3A). Compared with MOD group, lower TRAP activity, and less positive cells in both XAN groups (both $P < 0.01$) indicated that XAN decreased TRAP activity and inhibited OC differentiation, thus reducing bone destruction. The TRAP activity and positive cells in XAN-H group were lower than that in XAN-L group (Fig. 3B, $P < 0.01$), showing that its effect on bone destruction was positively correlated with the dosage of XAN. The above results suggested that XAN could remarkably reduce OC differentiation, inhibit osteoclastic activity, and fight against gouty bone injury.

Effects of XAN on expression of proteins related to bone metabolism

The number and density of CTSK, MMP-9 and MMP-13 positive cells in MOD group were higher than those in CON group (Fig. 4B–D, all $P < 0.01$), indicating that MSU stimulated the expression of proteins related to bone resorption, such as CTSK, MMP-9 and MMP-13. Meanwhile, the number and density of Runx2-positive cells in MOD group were lower than those in CON group (Fig. 4E, $P < 0.01$), showing that MSU inhibited the expression of proteins related to bone formation, such as Runx2. However, the number and density of CTSK, MMP-9 and MMP-13 positive cells in XAN-H group, XAN-L group and ETO group were lower than those in MOD group (Fig. 4B–D, all $P < 0.01$), suggesting that XAN decreased expression of CTSK, MMP-9 and MMP-13, and inhibited

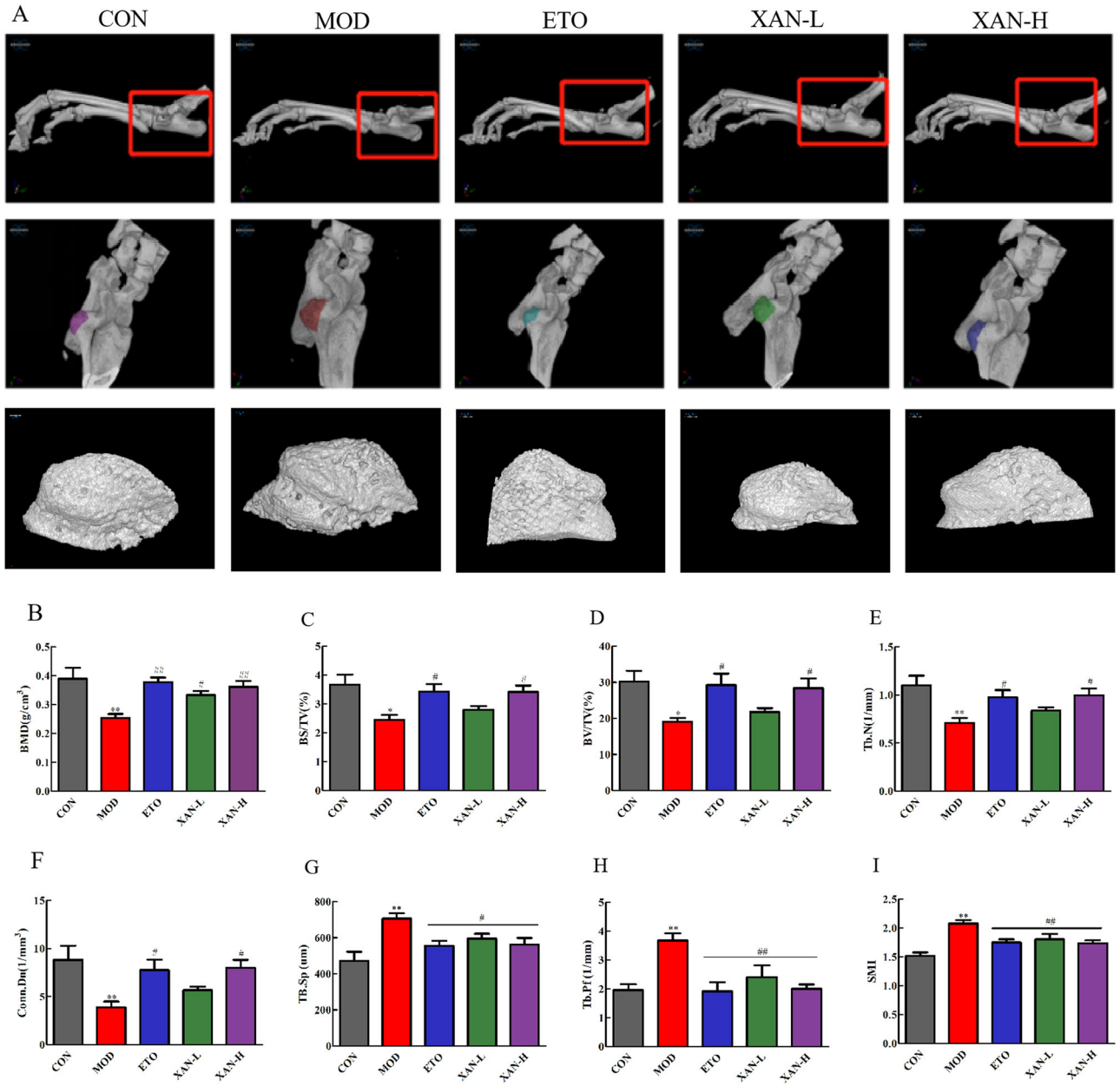

Fig. 2 Effects of XAN on bone morphology and parameters of joints. **A** Typical images of ankle joints. Red frame in plane indicates morphological changes of the lateral condyle and the fibula, while decreased bone density and increased fragility in MOD group. Colored parts in 3D map indicate ROI region for quantitative analysis of bone microparameters. ROI shows morphological changes of bone tissue in this area. There are obvious signs of bone damage as bone surface was uneven and even hollow in MOD group; scale bars = 100 μm; (**B**). BMD; (**C**). BS/TV; (**D**). BV/TV; (**E**). Tb. N.; (**F**). Conn.Dn.; (**G**). Tb. Sp.; (**H**). Tb. Pf.; (**I**). SMI. n=10, $\bar{x} \pm s$. $^{*}P < 0.05$, $^{**}P < 0.01$ vs. control group; $^{\#}P < 0.05$, $^{\#\#}P < 0.01$ vs. model group. 3D Three-dimensional, ROI region of interest, BMD bone mineral density, BS/BV bone surface/bone volume, BV/TV bone volume/tissue volume, Tb.N: trabecular number, Conn.Dn. Connectivity density, Tb.Sp. trabecular separation, Tb.Pf. trabecular bone pattern factor, SMI structural model index

bone destruction caused by MSU. The number and density of Runx2-positive cells in XAN-H group were higher than those in MOD group (Fig. 4E, $P < 0.05$), indicating that XAN at high dose increased bone formation in GA. The above results revealed that XAN could inhibit bone destruction and promote bone formation, thus regulating abnormal bone metabolism in GA.

Effects of XAN on RANKL/OPG Bone Metabolic Signaling Pathway

The number of RANKL and OPG positive cells and the ratio of RANK /OPG in MOD group were higher than those in CON group (Fig. 5, all $P < 0.01$), suggesting that MSU stimulated RANKL secretion, whereas OPG expression was

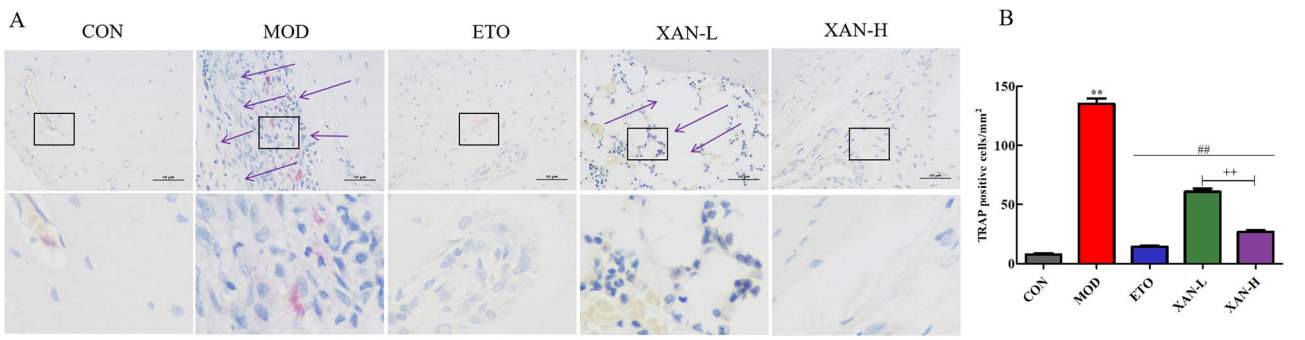

Fig. 3 Effects of XAN on differentiation of OC. **A** Representative images of TRAP staining, positive cells indicated with arrows, scale bars = 50 μm; (**B**) number of TRAP positive cells. $n = 10$, $\bar{x} \pm s$. $^{**}P < 0.01$ vs. CON group; $^{\#\#}P < 0.01$ vs. MOD group; $^{++}P < 0.01$ vs. XAN-L group. TRAP Tartrate resistant acid phosphatase

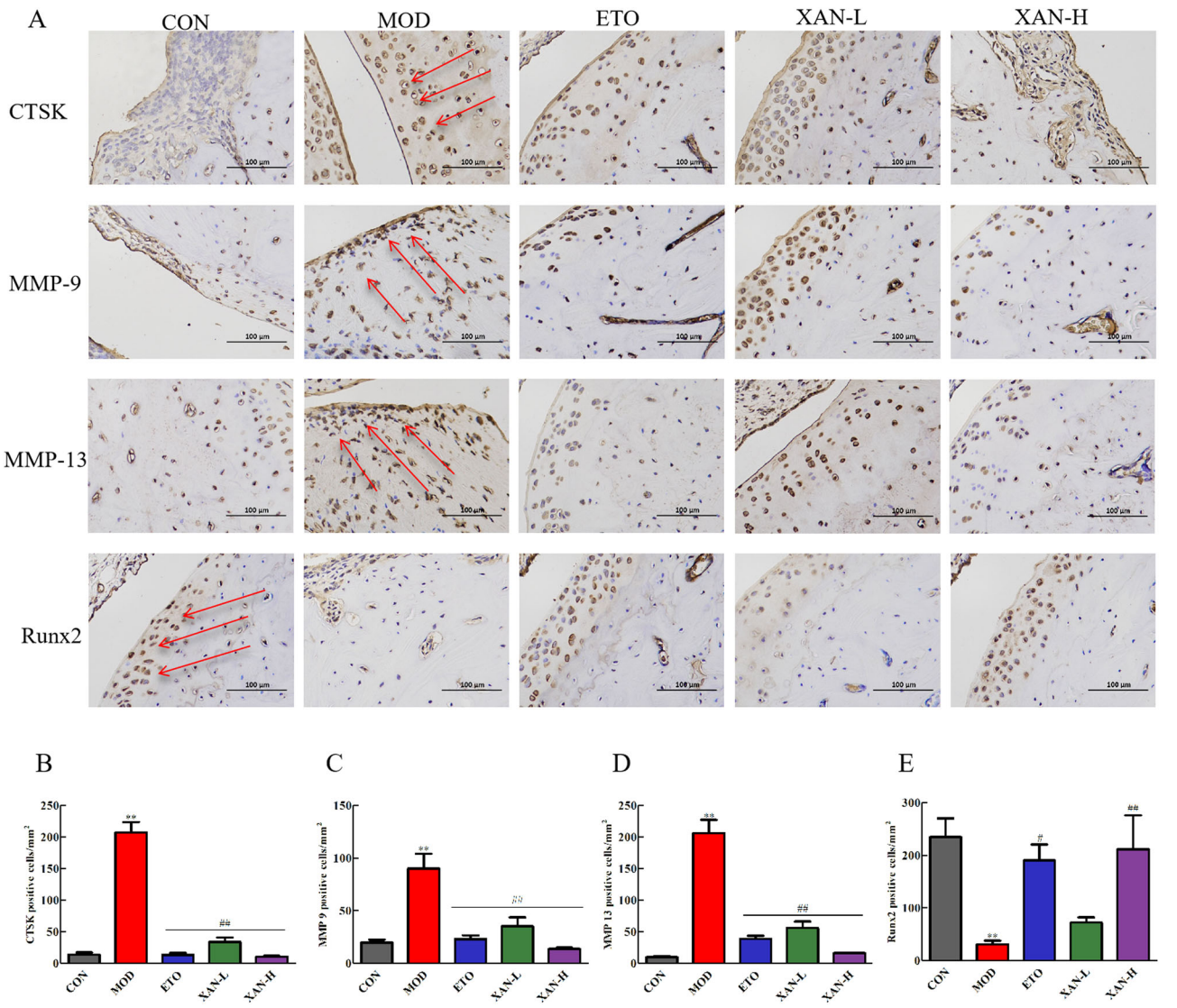

Fig. 4 Effects of XAN on expression of proteins related to bone metabolism. **A** Typical IHC staining, positive cells indicated with red arrows, scale bars = 100 μm; (**B**) CTSK; (**C**) MMP-9; (**D**) MMP-13; (**E**) Runx2. $n = 10$, $\bar{x} \pm s$. $^{**}P < 0.01$ vs. CON group; $^{\#}P < 0.05$, $^{\#\#}P < 0.01$ vs. MOD group; $^{+}P < 0.05$ vs. Abbreviations: IHC immunohistochemical, CTSK Cathepsin K, MMP matrix metalloproteinase, Runx2 Runt-related transcription factor 2

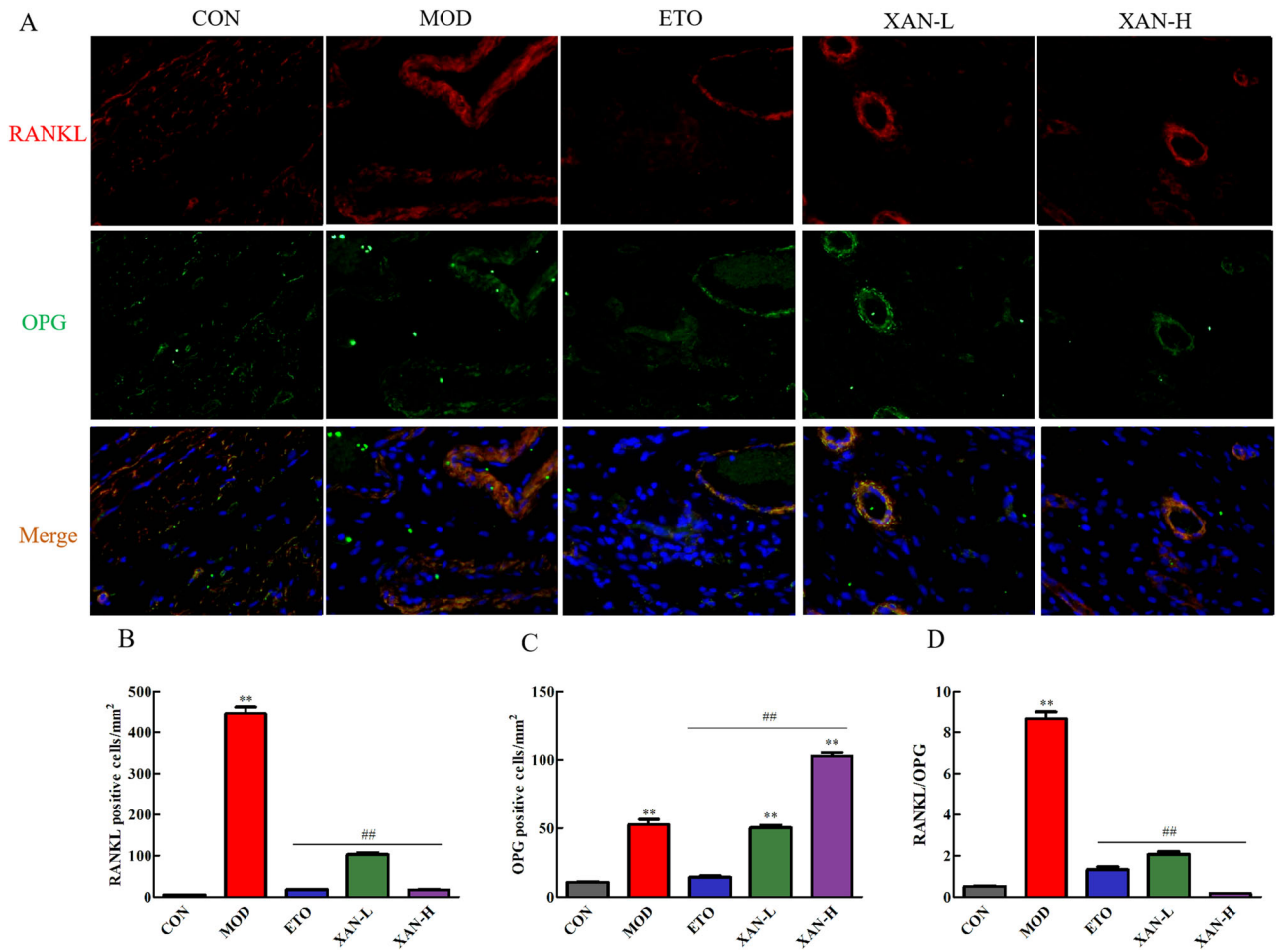

Fig. 5 Effects of XAN on RANKL/OPG bone metabolic signaling pathway. **A** Representative images of double-labeling immunofluorescent staining of RANKL (red), OPG (green) and merge co-localization (violaceous), scale bars = 100 μm; (**B**) RANKL; (**C**) OPG; (**D**). RANKL/OPG. $n = 10$, $\bar{x} \pm s$. $^{**}P < 0.01$ vs. CON group; $^{\#\#}P < 0.01$ vs. MOD group. RANKL recombinant receptor activator of nuclear factor kappa B ligand, OPG osteoprotogerin

passively up-regulated to maintain bone homeostasis by preventing excessive formation of complex with RANKL and RANK, thus inhibiting RANKL-induced OC differentiation. The increased ratio of RANKL/OPG indicated that bone destruction dominated the bone metabolic imbalance, which inferred that RANKL/OPG signaling pathway was activated by MSU. The number of RANKL-positive cells in XAN-H group, XAN-L group and ETO group were lower than those in MOD group (all $P < 0.01$), indicating that XAN inhibited RANKL secretion to reduce RANKL-induced OC differentiation, thus improving bone resorption in GA rats. The number of OPG positive cells in XAN-H group and XAN-L group were higher than those in CON group (all $P < 0.01$), and the number of OPG positive cells of XAN-H group was also higher than MOD group ($P < 0.01$), indicating that XAN had protective effect on bone with enhancing OPG expression to competitively inhibit OC differentiation. The ratio of RANKL/OPG in ETO group and XAN groups were lower than that in MOD group (all $P < 0.01$), suggesting that XAN could correct or even reverse the bone metabolic imbalance caused by MSU. The above results confirmed that the mechanism of XAN against gouty bone injury was related to its inhibition of RANKL/OPG bone metabolic signaling pathway.

Discussion

Anti-inflammation is primary principle of treatment in acute GA [31]. However, there are many defects with current clinical drugs, including toxicity of colchicine, side effects of glucocorticoid, gastrointestinal reaction of non-steroid anti-inflammatory drugs. This study revealed that XAN had good anti-inflammatory effect on GA rats, which could descend level of IL-1β, IL-6, TNF-α and PGE2, abate joint swelling, decrease Markin's score of ankle joint tissue, and improve gouty arthritis damage. Results also showed that XAN may be a good alternative for treating gout conditions

with nice tolerance, as long-term use without adverse reactions and side effects [18, 19], despite of the less efficacy compared to positive control ETO.

Meanwhile, this study also illustrated that XAN could fight against gouty bone damage different from inflammatory pathways, while other studies showed that common osteoarthritis led to bone destruction mostly due to activation of inflammatory pathways, like OC differentiation mediated by TNF-α [32]. As bone homeostasis is balanced with multiple signaling pathways to regulate bone resorption and bone formation, the mechanism of XAN against gouty bone injury should focus on bone metabolic signaling pathways independent of inflammation, such as RANKL/OPG, Wnt/β-Catenin, TGF-β/Smad and so on [33]. In this study, we firstly confirmed that XAN inhibited RANKL secretion, promotes expression of OPG, and corrected or even reversed the ratio of RANKL/OPG, thus promoting bone formation and inhibiting bone destruction via inhibition of RANKL/OPG signaling pathway to regulate bone homeostasis in GA rats. Concretely speaking, complex of RANKL and RANK recruited TRAF6, mitogen-activated protein kinases (MAPKs), transcription factor nuclear factor-κB (NF-κB) and activator protein-1 (AP-1), then activated NFATc1 [34]. Furthermore, NFATc1 was a key regulator leading to OC differentiation, and responsible for inducing expression of specific target genes and transcription factors in OC differentiation. Moreover, massive secretion of proteins related to bone resorption, including TRAP and CTSK, were stimulated to participate in the process of OC differentiation and maturation, thus promoting proliferation and inhibiting apoptotic [35–37]. In addition, we also confirmed that XAN inhibited TRAP activity, descended OC differentiation, and decreased the expression of proteins involved in bone resorption, such as CTSK. Meanwhile, our results also showed that XAN prevented excessive differentiation of OC by increasing expression of OPG, which was associated with OPG competitive binding to RANKL leading to less formation of RANK-RANKL complex [38]. Therefore, we concluded that XAN fought against gouty bone injury by targeting RANKL/OPG/RANK bone metabolic signaling pathway.

Above all, this study innovatively confirmed that XAN had anti-inflammatory and anti-bone injury effects in GA rats, and preliminarily proved that its mechanism of anti-gouty bone injury is related to the inhibition of RANKL/OPG/RANK bone metabolic signaling pathway.

Certainly, the mechanisms of bone metabolism are very complex and targets involved in pathways are so many. Although this study confirms that XAN plays a regulatory role through RANKL/OPG/RANK signaling pathway, other targets of this signaling pathway have not been explored yet. Therefore, further study is still needed on whether XAN can activate other targets.

Conclusion

In conclusion, our findings about effects of XAN against gouty bone damage and its mechanism via RANKL/OPG/RANK signaling pathway are innovative until now, which further provides reference for clinical application. Therefore, we recommend XAN as a beneficial therapeutic strategy for protective treatment in GA and support further researches investigated for resource development of *Humulus lupulus* L.

Author Contributions J.H.: Writing—original draft, Investigation, Formal analysis, Conceptualization. T.X.: Writing—review & editing, Supervision, Project administration. Y.J.: Supervision, Conceptualization. W.F.: Data curation, Software, Methodology. N.W.: Visualization, Methodology. Y.Z.: Writing—review & editing, Formal analysis. A.L.: Writing—review & editing. K.Z.: Writing—review & editing. H.X.: Project administration, Methodology, Funding acquisition. All authors reviewed the manuscript.

Funding This work was supported by the National Natural Science Foundation of China (82174079), Project of Science and Technology Commission of Shanghai Municipality (21S21902600).

Compliance with Ethical Standards

Conflict of Interest The authors declare no competing interests.

Ethical Approval The animal studies reported in this manuscript were carried out in accordance with local ethical guidelines for animal experiments issued by the Naval Medical University, and were approved by the Committee on Ethics of Medical Research (approved No. 202102624).

References

1. Huddleston, E. M., & Gaffo, A. L. (2022). Emerging strategies for treating gout. *Current Opinion in Pharmacology*, *65*, 102241. https://doi.org/10.1016/j.coph.2022.102241.
2. Singh, J. A., & Gaffo, A. (2020). Gout epidemiology and comorbidities. *Seminars in Arthritis and Rheumatism*, *50*, S11–S16. https://doi.org/10.1016/j.semarthrit.2020.04.008.
3. Feng, W., & Xiong, G. (2021). Clinical classification and treatment experience of wrist gouty arthritis. *Chinese Journal of Reparative and Reconstructive Surgery*, *35*, 1411–1416. https://doi.org/10.7507/1002-1892.202103043.
4. Gelber, A. C.(2022). Treatment guidelines in gout. *Rheumatic Disease Clinics of North America*, *48*, 659–678. https://doi.org/10.1016/j.rdc.2022.04.003.
5. Blake, K. E. G., Saag, J. L., & Saag, K. G. (2022). What's new on the front-line of gout pharmacotherapy?. *Expert Opinion on Pharmacotherapy*, *23*, 453–464. https://doi.org/10.1080/14656566.2021.2020249.
6. Bafna, P. S., Patil, P. H., Maru, S. K., & Mutha, R. E. (2021). Cissus quadrangularis L: A comprehensive multidisciplinary review. *Journal of Ethnopharmacology*, *279*, 114355. https://doi.org/10.1016/j.jep.2021.114355.
7. Al Mamun, M. A., Hosen, M. J., & Islam, K. et al.(2015). Tridax procumbens flavonoids promote osteoblast differentiation and

bone formation. *Biological Research*, *48*, 65. https://doi.org/10.1186/s40659-015-0056-1.
8. Al Mamun, M. A., Islam, K., & Alam, M. J. et al.(2015). Flavonoids isolated from Tridax procumbens (TPF) inhibit osteoclasts differentiation and bone resorption. *Biological Research*, *48*, 51. https://doi.org/10.1186/s40659-015-0043-6.
9. Feng, W., Zhong, X. Q., & Zheng, X. X. et al.(2022). Study on the effect and mechanism of quercetin in treating gout arthritis. *International Immunopharmacology*, *111*, 109112. https://doi.org/10.1016/j.intimp.2022.109112.
10. Qiao, C. Y., Li, Y., & Shang, Y., et al. (2020). Management of Gout-associated MSU crystals-induced NLRP3 inflammasome activation by procyanidin B2: targeting IL-1β and Cathepsin B in macrophages. *Inflammopharmacology*, *28*, 1481–1493. https://doi.org/10.1007/s10787-020-00758-8.
11. Zhao, Z., Luo, J., & Liao, H. et al.(2023). Pharmacological evaluation of a novel skeleton compound isobavachin (4',7-dihydroxy-8-prenylflavanone) as a hypouricemic agent: Dual actions of URAT1/GLUT9 and xanthine oxidase inhibitory activity. *Bioorganic Chemistry*, *133*, 106405. https://doi.org/10.1016/j.bioorg.2023.106405.
12. Aggarwal, D., Upadhyay, S. K., Singh, R., & Tuli, H. S. (2021). Recent patents on therapeutic activities of xanthohumol: a prenylated chalconoid from hops (Humulus lupulus L). *Pharmaceutical Patent Analyst*, 10, 37–49. https://doi.org/10.4155/ppa-2020-0026.
13. Vicente de Andrade Silva, G., Demaman Arend, G., & Antonio Ferreira Zielinski, A., et al. (2023). Xanthohumol properties and strategies for extraction from hops and brewery residues: A review. *Food Chemistry*, *404*, 134629. https://doi.org/10.1016/j.foodchem.2022.134629.
14. Deng, P., Wang, S., & Sun, X. et al.(2022). Global trends in research of gouty arthritis over past decade: A bibliometric analysis. *Frontiers in Immunology*, *13*, 910400. https://doi.org/10.3389/fimmu.2022.910400.
15. Liu, M., Hansen, P. E., & Wang, G., et al. (2015). Pharmacological profile of xanthohumol, a prenylated flavonoid from hops (*Humulus lupulus* L.). *Molecules*, *20*, 754–779. https://doi.org/10.3390/molecules20010754.
16. Tuli, H. S., Aggarwal, V., & Parashar, G. et al.(2022). Xanthohumol: A metabolite with promising anti-neoplastic potential. *Anti-Cancer Agents in Medicinal Chemistry*, *22*, 418–432. https://doi.org/10.2174/1871520621666210223095021.
17. van Breemen, R. B., Yuan, Y., & Banuvar, S. et al.(2014). Pharmacokinetics of prenylated hop phenols in women following oral administration of a standardized extract of hops. *Molecular Nutrition & Food Research*, *58*, 1962–1969. https://doi.org/10.1002/mnfr.201400245.
18. Dorn, C., Bataille, F., Gaebele, E., Heilmann, J., & Hellerbrand, C. (2010). Xanthohumol feeding does not impair organ function and homoeostasis in mice. *Food Chemistry Toxicology*, *48*, 1890–1897. https://doi.org/10.1016/j.fct.2010.04.030.
19. Hussong, R., Frank, N., & Knauft, J. et al.(2005). A safety study of oral xanthohumol administration and its influence on fertility in Sprague Dawley rats. *Molecular Nutrition & Food Research*, *49*, 861–867. https://doi.org/10.1002/mnfr.200500089.
20. Langley, B. O., Joan, J. R., & Douglas, H., et al. (2021). Xanthohumol microbiome and signature in healthy adults (the XMaS Trial): Safety and tolerability results of a phase I triple-masked, placebo-controlled clinical trial. *Molecular Nutrition & Food Research*, *65*, e2001170–e2001170. https://doi.org/10.1002/MNFR.202001170.
21. Han, J. Y., Xia, T. S., & Jiang, Y. P., et al. (2024). Regulation of xanthohumol on serum uric acid level and bone metabolism in hyperuricemia rats. *Academic Journal of Naval Medical University*, *45*, 260–267. https://doi.org/10.16781/j.CN31-2187/R.20230636.
22. Bai, H. H., Xia, T. S., & Jiang, Y. P., et al. (2022). Absorption, metabolism, and pharmacokinetic profile of xanthohumol in rats as determined via UPLC-MS/MS. *Biopharm Drug Dispos*, *43*, 11–22. https://doi.org/10.1002/bdd.2306.
23. Sun, X. L., Zhang, J. B., & Guo, Y. X. et al.(2021). Xanthohumol ameliorates memory impairment and reduces the deposition of β-amyloid in APP/PS1 mice via regulating the mTOR/LC3II and Bax/Bcl-2 signalling pathways. *Journal of Pharmacy and Pharmacology*, *73*, 1230–1239. https://doi.org/10.1093/jpp/rgab052.
24. Sun, X., Xia, T. & Zhang, S. et al.(2022). Hops extract and xanthohumol ameliorate bone loss induced by iron overload via activating Akt/GSK3β/Nrf2 pathway. *The Journal of Bone and Mineral Metabolism*, *40*, 375–388. https://doi.org/10.1007/s00774-021-01295-2.
25. Xia, T., Liu, X., & Wang, N. et al.(2022). PI3K/AKT/Nrf2 signalling pathway is involved in the ameliorative effects of xanthohumol on amyloid β-induced oxidative damage and bone loss. *Journal of Pharmacy and Pharmacology*, *74*, 1017–1026. https://doi.org/10.1093/jpp/rgac007.
26. Xia, T. S., Lin, L. Y., & Zhang, Q. Y. et al.(2021). *Humulus lupulus* L. extract prevents ovariectomy-induced osteoporosis in mice and regulates activities of osteoblasts and osteoclasts. *Chinese Journal of Integrative Medicine*, *27*, 31–38. https://doi.org/10.1007/s11655-019-2700-z.
27. Yan, F., Zhang, H., & Yuan, X. et al.(2023). Comparison of the different monosodium urate crystals in the preparation process and pro-inflammation. *Advances in Rheumatology*, *63*, 39. https://doi.org/10.1186/s42358-023-00307-1.
28. Lin, Y. Y., Jean, Y. H., & Lin, S. C. et al.(2020). Etoricoxib prevents progression of osteolysis in repeated intra-articular monosodium urate-induced gouty arthritis in rats. *Journal of Advanced Research*, *24*, 109–120. https://doi.org/10.1016/j.jare.2020.02.014.
29. Sunk, I. G., Amoyo-Minar, L., & Niederreiter, B. et al.(2022). Dorso-ventral osteophytes of interphalangeal joints correlate with cartilage damage and synovial inflammation in hand osteoarthritis: a histological/radiographical study. *Arthritis Research & Therapy*, *24*, 226. https://doi.org/10.1186/s13075-022-02911-w.
30. Crowe, A., & Yue, W. (2023). Update notice: Semi-quantitative determination of protein expression using immunohistochemistry staining and analysis. *Bio-protocol*, *13*, e4610. https://doi.org/10.21769/BioProtoc.4610.
31. Banerjee, M., & Mukhopadhyay, S. (2023). Gout. *The New England Journal of Medicine*, *388*, 47. https://doi.org/10.1056/NEJMc2216467.
32. Yokota, K.(2024). Osteoclast differentiation in rheumatoid arthritis. *Immunological Medicine*, *47*, 6–11. https://doi.org/10.1080/25785826.2023.2220931.
33. Patil, T., Soni, A., & Acharya, S. (2021). A brief review on in vivo models for Gouty Arthritis. *Metabol Open*, *11*, 100100. https://doi.org/10.1016/j.metop.2021.100100.
34. Li, Z., Li, D., & Chen, R. et al.(2023). Cell death regulation: A new way for natural products to treat osteoporosis. *Pharmacological Research*, *187*, 106635. https://doi.org/10.1016/j.phrs.2022.106635.
35. Liu, Y., Song, F. M., & Ma, S. T. et al.(2019). Vaccarin prevents titanium particle-induced osteolysis and inhibits RANKL-induced osteoclastogenesis by blocking NF-κB and MAPK signaling pathways. *Journal of Cellular Physiology*, *234*, 13832–13842. https://doi.org/10.1002/jcp.28063.
36. Park, J. H., Lee, N. K., & Lee, S. Y. (2017). Current understanding of RANK signaling in osteoclast differentiation and maturation. *Molecular Cell*, *40*, 706–713. https://doi.org/10.14348/molcells.2017.0225.

37. Wu, Z., Wu, H., & Li, C. et al.(2019). Daphnetin attenuates LPS-induced osteolysis and RANKL mediated osteoclastogenesis through suppression of ERK and NFATc1 pathways. *Journal of Cellular Physiology*, *234*, 17812–17823. https://doi.org/10.1002/jcp.28408.
38. Kim, J. M., Lin, C., & Stavre, Z., et al. (2020). Osteoblast-osteoclast communication and bone homeostasis. *Cells*, *9*, 2073. https://doi.org/10.3390/cells9092073.